Appl Phys A (2012) 107:761–767
DOI 10.1007/s00339-012-6921-7

Applied Physics A
Materials Science & Processing

RAPID COMMUNICATION

Spontaneous wrinkling pattern of a constrained thin film membrane

Yuan Yan · Binglei Wang · Jie Yin · Tiejun Wang · Xi Chen

Received: 5 May 2011 / Accepted: 4 April 2012 / Published online: 18 April 2012

Abstract The wrinkling morphology of an inhomogeneously constrained thin film membrane is explored using finite element simulations, where a small circular area in a thin sheet undergoes expansion, and buckles emerge due to differential in-plane deformation. The local wrinkling patterns are characterized by the normalized circular (inner) area size, the modulus mismatch between the inner and outer regions, and the normalized stress in the inner area. As the stress increases, the morphology transits from ripple-like to petal-like and finally to a branched pattern. Through parametric studies, the effect of the governing variables on the pattern evolution, wave number, and maximum deflection is discussed. The model is used to qualitatively explain the delamination/blister morphology observed in thin film/substrate systems. The study has the potential of inspiring new fabrication techniques based on mechanical self-assembly.

Y. Yan · T. Wang
School of Aerospace, Xi'an Jiaotong University, Xi'an 710049, China

B. Wang · J. Yin · X. Chen (✉)
Department of Earth and Environmental Engineering, Columbia University, New York, NY 10027, USA
e-mail: xichen@columbia.edu

B. Wang
Department of Engineering Mechanics, Shandong University, Jinan, Shandong 250061, China

X. Chen
International Center for Applied Mechanics, SV Lab, Xi'an Jiaotong University, Xi'an 710049, China

X. Chen
Department of Civil & Environmental Engineering, Hanyang University, Seoul 133-791, Korea

1 Introduction

Wrinkling patterns of thin sheets are ubiquitous, including those observed along the edge of torn plastic sheets, in clothes and free hanging curtains, in a piece of crumpled paper, and in cream films floating on warm milk [1]. The exploration of the underlying mechanics has attracted increasing interest.

Mismatched deformation is an effective way to induce the formation of wrinkles in thin sheets. In some cases, the mismatched deformation relies on an underlying aqueous foundation. For instance, Huang et al. [2] reported the wrinkling of a freely floating polymer sheet driven by capillary force, and the scaling relationship between the capillary load and the geometry of wrinkles was revealed. Similarly, when a floating polyester sheet on water was compressed, Pocivavsek et al. [3] observed the transition from wrinkles to folds upon further compression. In some other cases, the mismatched deformation results from boundary constraint. For example, when a container with a piece of paper inside is shrunk, the paper becomes crumpled and sharp vertices and ridges are developed in the paper. The crumpling of elastic and plastic sheets under confinement has been extensively investigated [1, 4, 5].

In the category of pressure-driven deformation of a thin sheet, bulge test has been widely employed in the characterization of mechanical properties. For instance, Small and Nix [6] developed a set of equations for analyzing bulge test data of a constrained circular thin film. This was later extended to square and rectangle thin films [7]. Recently, strain gradient theory was introduced for explaining the bulge test data [8].

For those freestanding thin films without external constraints or pressure, wrinkling requires inhomogeneous deformation. Cerda and Mahadevan [9] studied the wrinkling

of stretched thin elastic sheets and revealed the general scaling law on the wavelength of wrinkles through the minimization of the total energy. Sharon et al. [10] found that the superposition of short wave length mode leads to the multiscale wrinkling patterns along the edge of torn plastic sheets. By differentially stretching a foam ribbon, the instability could reproduce the typical shape of a long leaf, saddle-like in the center and wavy in the edge [11]. The relevant mechanism has been used to explain the morphogenetic processes of some plants. For example, when the local growth rate at the edge of an eggplant leaf was faster, a normally flat leaf could buckle into a wavy one [12]. Similarly, when a soft swelling gel corona was clamped to the edge of a disk of a stiff nonswelling gel, buckling occurred upon swelling and out-of-plane wavy edges were formed [13], which was employed to qualitatively explain the shape of a leaf [14]. Besides plant morphology, the spontaneous instability of a thin sheet provides an alternative technique for manufacturing. For instance, for a thin gel sheet that is initially flat, through the programmed control of the local swelling or shrinkage in the elastic sheets, the nonuniform deformation could lead to the formation of a variety of 3D global non-Euclidean structures via buckling [15, 16].

In most of these previous studies involving inhomogeneous deformation, the excessive strain occurs near the perimeter, leading to wrinkles at the edge of a thin film membrane. In this paper, we consider an alternative case where the local wrinkles occur in the center of a thin sheet. For example, when a drop of water is accidentally spilled in the middle of a piece of hydrophilic paper, the fiber structure in the small hydrated area becomes relaxed and more compliant than its surrounding, and the swelling induced by hydrogen bond in the soggy area renders itself in compression (owing to the constraint of the surrounding area) to form an intriguing spontaneous out-of-plane wrinkle pattern. Similar phenomenon is also often observed in paint upon local swelling (e.g. by a drop of toluene) [17]. Motivated by this common phenomenon, we explore the pattern evolution of an inhomogeneously deformed thin sheet, where a small expanding and compliant local area is constrained by its surroundings. Besides providing some useful insights on the interesting morphology of wetted paper and explaining the thin film delamination patterns, the study may also inspire new manufacturing routes by taking advantage of the self-assembled instabilities.

2 Model and method

Consider a large circular thin sheet with thickness t and outer radius R (Fig. 1). The inner circular region with radius r is allowed to expand/swell to mimic the hydrogen bond-induced wetting process. Since the thin sheet is hydrophilic, the effect of capillary force on the wrinkling process is neglected. We neglect liquid diffusion and assume r to be fixed in the due course of wrinkling. Thus, by assuming the in-plane compressive stress to be the main driving force of wrinkling, the present study can be extended to many other similar self-assembled instability problems without water (capillary force), discussed below.

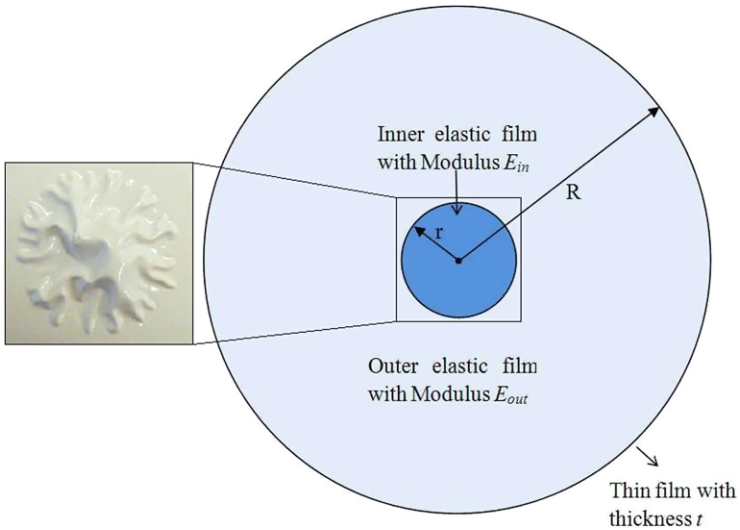

Fig. 1 Schematic illustration of the wrinkling model of a membrane thin sheet that undergoes differential in-plane deformation. The sheet thickness is t; its inner region (which subjects to in-plane swelling/expansion) has a fixed radius r and elastic modulus E_{in}; the outer region has radius R and elastic modulus E_{out} (with $r \ll R$ and $E_{\text{in}} \leq E_{\text{out}}$). The constrained swelling renders the inner area in compression, which leads to various wrinkling patterns depending on the stress level in the film, the normalized inner region size r/t, and the modulus ratio $E_{\text{in}}/E_{\text{out}}$. The *left illustration* is from Ref. [17]

The modulus of the inner and outer region is E_{in} and E_{out}, respectively. The Poisson's ratio (v) and the sheet thickness are assumed to be uniform. When the inner region experiences a mismatched in-plane equibiaxial strain $\Delta\varepsilon$, based on the continuity of the displacement at the interface between the inner and outer regions, it is straightforward to derive the magnitude of the pre-buckling compressive stress in the inner area:

$$\sigma_f = \sigma_r = \sigma_\theta = \frac{E_{\text{out}}E_{\text{in}}(R^2 - r^2)\Delta\varepsilon}{E_{\text{out}}(1-v)(R^2-r^2) + E_{\text{in}}[(v-1)r^2 + (1+v)R^2]} \quad (1)$$

In our current problem of focus, the inner region is very small so as to minimize the edge effect, and when $r/R \ll 1$, the pre-buckling stress reduces to

$$\sigma_f = \frac{E_{\text{out}}E_{\text{in}}\Delta\varepsilon}{E_{\text{out}}(1-v) + E_{\text{in}}(1+v)} \quad (2)$$

The stress in the inner region continues to arise with $\Delta\varepsilon$, and when it exceeds a critical value σ_c, instability occurs. The constrained elastic wrinkling model is investigated numerically using the commercial software ABAQUS, where the membrane thin film is discretized by over 25,000 4-node general purpose shell elements with reduced integration and accounting for large rotation. Only rigid body motion is constrained at the edge of outer area. The swelling inner area, as well as the interface between the inner and outer areas, is finely meshed. The first buckling eigenmode calculated from elastic buckling analysis is used as the shape template of the small initial defect, so as to facilitate the out-of-plane buckling. The magnitude of the initial imperfection is kept below 1 % of the sheet thickness to ensure that it has no effect on the final wrinkling morphology.

3 Results and discussion

In this study, we focus on the buckle pattern within the inner region: although sometimes the crumples may extend radially into the outer region, such undulation decays quickly especially when $E_{\text{out}}/E_{\text{in}}$ is high. From dimensional analysis [18, 19], the characteristics of the wrinkles are primarily governed by several dimensionless parameters, σ_f/σ_c, r/t, and $E_{\text{out}}/E_{\text{in}}$.

3.1 Wrinkling map: effect of stress level

We first investigate the effect of stress level σ_f/σ_c on the evolution of the wrinkling patterns. In Fig. 2(a), a map of wrinkling patterns is shown for different normalized membrane sizes and stress levels, where the modulus mismatch is fixed as $E_{\text{out}}/E_{\text{in}} = 20$. While in Fig. 2(b), a map is given for different modulus mismatch ratios and stress levels, where the normalized membrane size $r/t = 500$ is considered. Qualitatively, all buckled morphologies can be divided into three major categories in the present study: (1) ripple pattern, (2) petal pattern, and (3) branched pattern. The ripple pattern appears just above critical $\sigma_f/\sigma_c = 1$ and more radial ripple waves form with larger constrained membrane size. With the increase of stress level the circumferential wrinkles emerge, and the petal pattern is formed. The dashed curve in Fig. 2 is an approximate boundary between the ripple and petal patterns. When the stress level becomes relatively high, the end of petals splits and the branched pattern occurs as a higher order mode; the branched pattern is favored for a constrained membrane with larger size (r/t) and higher compliance ($E_{\text{out}}/E_{\text{in}}$). The solid curve in Fig. 2 roughly separates the petal and the branched patterns with different parameters.

In essence, both global out-of-plane deflection and local wrinkling are involved in the instability process. At the onset of buckling (with σ_f/σ_c just above 1), the inner region first loses stability and triggers the ripple waves, and the radial stress is partially relieved. When σ_f/σ_c gets higher, to effectively release the hoop stress the radial petal-like mode is preferred. When the stress is even higher, more waves are required to minimize the strain energy: hence the branched pattern. Figure 2 also suggests that in case of very large r/t or $E_{\text{out}}/E_{\text{in}}$, the petal mode may be extinct, that is, if the constrained membrane film is very large or very compliant, after initial ripple wrinkling, with continued swelling the film buckle may become branched directly.

To further investigate the evolution of patterns at different stress levels, the variations of the normalized out-of-plane deflection (H/t) across the diameter of the inner region are given in Fig. 3. In all cases the cross section at which the overall deflection is the most prominent is selected. The geometrical and material parameters are $r/t = 300$ and $E_{\text{out}}/E_{\text{in}} = 20$, respectively. In the beginning when the stress is low (e.g. with σ_f/σ_c just above 1), the initially flat inner region loses its stability and buckles into the undulating sinusoidal waves (ripple pattern). With increased mismatch strain, the inner region bends outwards and the maximum out-of-plane displacement increases. The out-of-plane deflection primarily relieves the radial stress, and when the hoop stress becomes more critical, the petal waves appear at the circumferential edge. With higher stress level eventually the branched pattern appears; further increasing the stress level does not seem to alter the overall branched morphology (the number of wrinkles along hoop direction keeps fixed), although the maximum deflection keeps increasing slowly, which will be discussed later.

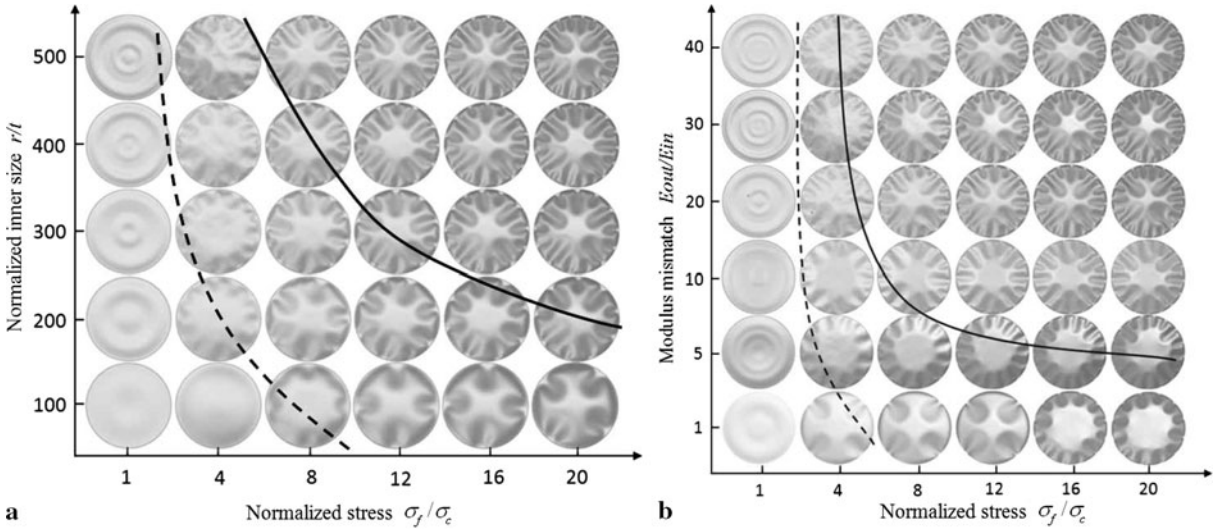

Fig. 2 Effect of the normalized stress σ_f/σ_c on the wrinkling patterns, with different normalized inner area size and modulus mismatch. (**a**) The modulus mismatch $E_{out}/E_{in} = 20$. (**b**) The normalized inner area size $r/t = 500$. Three types of patterns are formed when σ_f/σ_c increases: (i) the ripple pattern with concentric rings of buckles; (ii) the petal pattern; (iii) the branched pattern which is evolved from the petal pattern. The *dashed curve* separates (i) and (ii), and the *solid curve* separates (ii) and (iii)

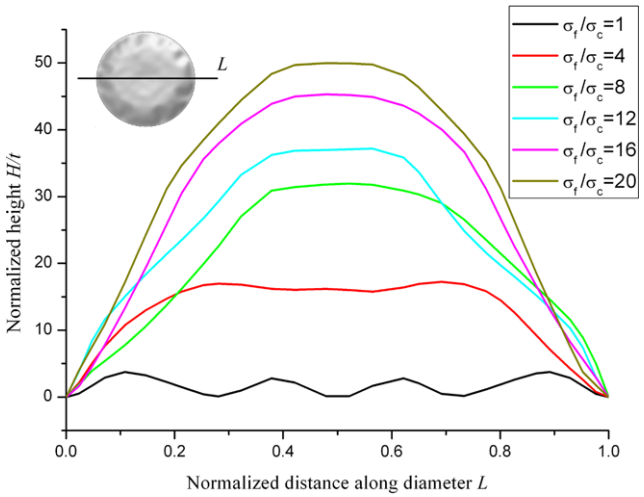

Fig. 3 Cross section profiles at different σ_f/σ_c for $r/t = 300$ and $E_{out}/E_{in} = 20$

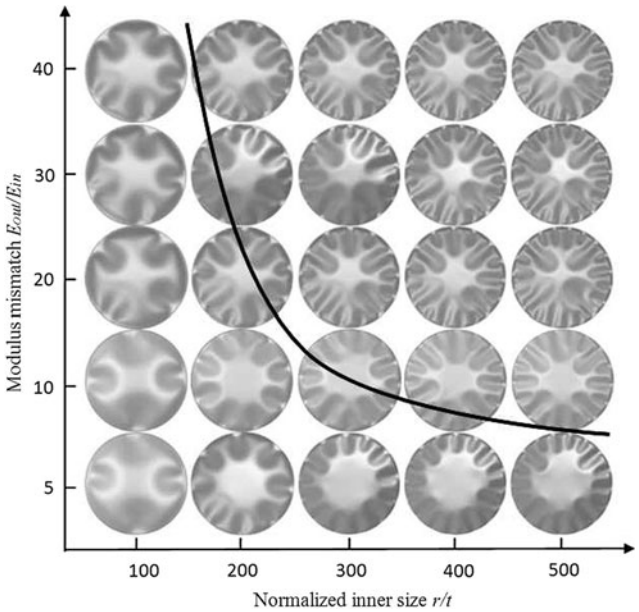

Fig. 4 Map of wrinkling patterns for different modulus mismatch E_{out}/E_{in} and normalized inner area size r/t, at $\sigma_f/\sigma_c = 20$. The *solid curve* approximately separates the petal patterns from the branched ones

3.2 Effect of geometrical and material parameters

The effect of the normalized inner region size r/t and the modulus mismatch E_{out}/E_{in} is given in Fig. 4. Without losing generality, the stress level is fixed at $\sigma_f/\sigma_c = 20$. For smaller r/t, the petal pattern is favored; otherwise the branched pattern takes over. The solid curve in Fig. 4 roughly separates the petal patterns from the branched patterns at the present stress level. The similar trend is also found for the effect of modulus mismatch; if E_{out}/E_{in} is low, the formation of branched patterns becomes difficult unless the stress is very high. In essence, for larger r/t and E_{out}/E_{in}, the bending stiffness of the inner region is relatively small, and it is easier to wrinkle at the same stress level.

3.3 Circumferential wrinkle wave number and center deflection

The two critical quantitative measures of the wrinkle profile are: the wavelength of the circumferential wrinkles, λ, mea-

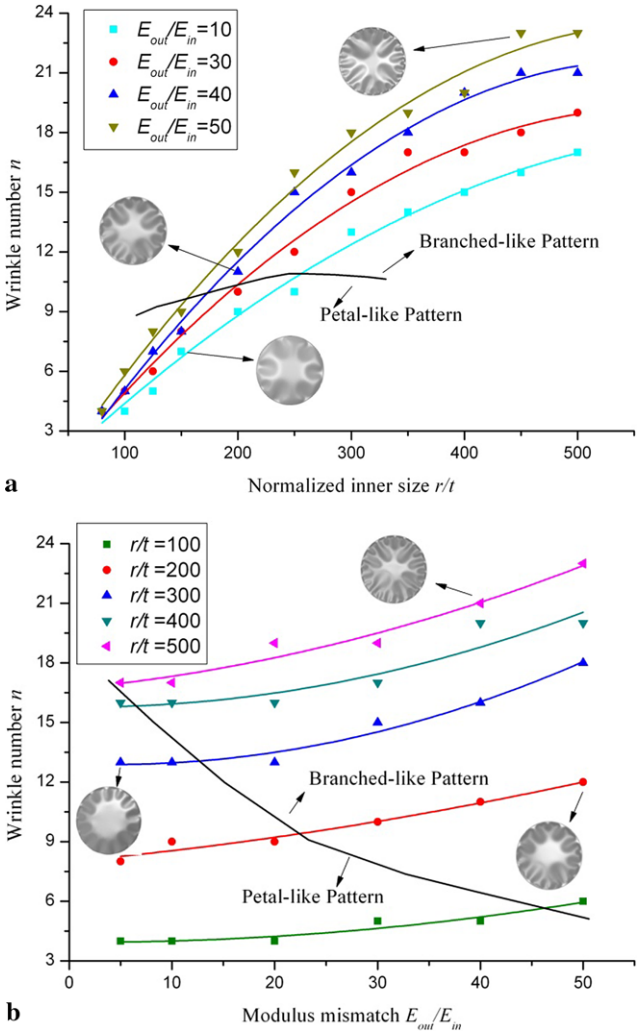

Fig. 5 Effect of normalized inner area size r/t and modulus mismatch $E_{\text{out}}/E_{\text{in}}$ on the wrinkle number n. (**a**) Effect of r/t on n with different $E_{\text{out}}/E_{\text{in}}$; (**b**) Effect of $E_{\text{out}}/E_{\text{in}}$ on n with different r/t

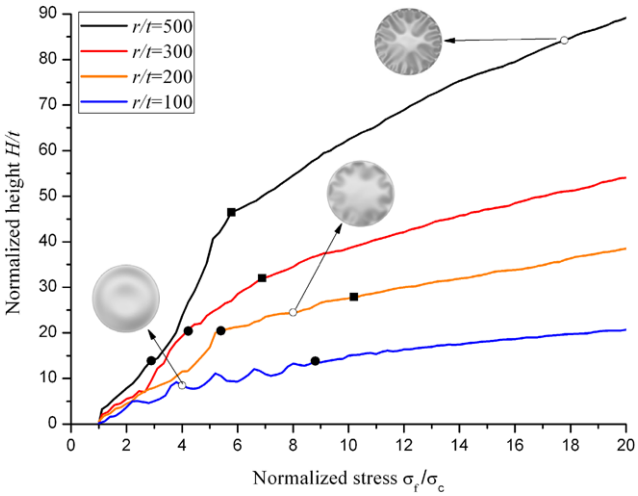

Fig. 6 Variation of the normalized center height H/t with different normalized stress, and for different r/t. The *black solid circles* separate the ripple patterns from petal ones; while the *black solid squares* denote the transition from petal to branched patterns

sured around the rim of the inner region (or equivalently the wrinkle number n with $n = 2\pi r/\lambda$); and the height of dome center, H.

For the wrinkle number plotted in Fig. 5, the stress is fixed at a relatively high level of $\sigma_f/\sigma_c = 20$. Figure 5 shows that the wrinkle number increases with the normalized inner area size and modulus mismatch. At low r/t, the wrinkle number is not very sensitive to the variation of $E_{\text{out}}/E_{\text{in}}$; meanwhile the difference becomes larger with a larger membrane size. Such a trend is consistent with the delamination experiment in literature which will be discussed later. The black curves in Fig. 5(a) and (b) approximately separate the petal patterns from branched patterns: again, the petal patterns occur with lower r/t and $E_{\text{out}}/E_{\text{in}}$, otherwise the branched patterns are preferred with more circumferential wave numbers.

In Fig. 6, the evolution of the deflection of the center of the membrane with respect to the normalized stress is demonstrated for four typical values of r/t, where the mismatch is fixed as $E_{\text{out}}/E_{\text{in}} = 40$. In general, the deflection is larger at a higher stress level and also for membranes with a larger size r/t. For the smallest film with $r/t = 100$, the center deflection oscillates with stress when the pattern is ripple-like. When the size of the constrained thin film membrane is moderately large, H/t increases almost monotonically with σ_f/σ_c. On each curve, the black solid circle denotes the transition from a ripple to a petal pattern, whereas the black solid square indicates the change from a petal to a branched pattern; in general, as r/t gets larger, the transition occurs at a lower normalized stress level yet with higher H/t. While H/t is quite sensitive to r/t, it is essentially insensitive to $E_{\text{out}}/E_{\text{in}}$ if r/t is fixed.

3.4 Comparison with delamination experiments

As remarked earlier, the present study has the potential of explaining the morphology of water-drop wetted paper, and inspiring new manufacturing techniques based on self-assembled wrinkles in constrained thin sheets. The detailed experimental studies will be reported in future. Meanwhile we note that the similar petal and branched patterns have been observed in delaminating blisters and detaching bubbles in film/substrate systems [17, 20, 21]. Although the mechanism of film buckle delamination is distinct from that in the current investigation, the findings in this paper may still provide some qualitative explanations on the overall morphology of these blisters.

Recently Lee et al. [21] studied the detachments of amorphous silicon (a-Si) membrane with $t = 300$ nm from an oxidized wafer (SiO_2/Si) substrate, by dissolving the sandwiched layer using hydrofluoric acid solution (HF/H_2O).

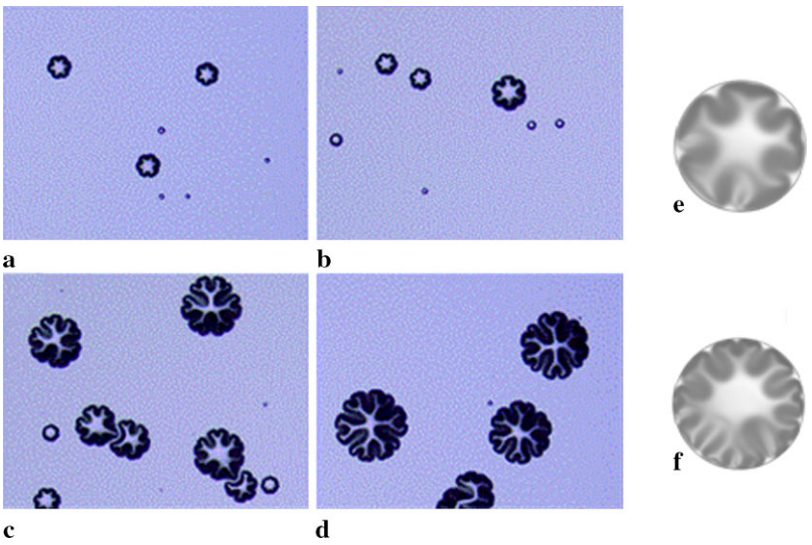

Fig. 7 Experimental observations of petal and branched patterns in detached blisters from substrates. (**a**)–(**d**) The wrinkling evolution of a growing amorphous silicon bubble detached from a substrate [21]. When the detached area is relatively small (**a**–**b**), petal morphology occurs with radial wrinkles around the rim. With further increasing of the detached area (**c**–**d**), branched morphology emerges with more waves at the rim. (**e**)–(**f**) Simulated petal and branched patterns using the present thin film model, at effective stress levels and blister sizes

The evolving patterns with the increase of dissolved area are shown in Fig. 7. Two possible triggers of the delamination were proposed: (1) the intrinsic residual compressive stress induced during the film deposition process, and (2) the upward lifting and radial stretching effect in the bubble caused by the underlying gaseous and liquid droplet inside the bubble. It was estimated that if the second factor is removed, the blister size may reduce by about 57 % [21]. The petal patterns (Fig. 7(a)–(b)) and branched patterns (Fig. 7(c)–(d)) were observed as the film buckle delaminates, whose normalized size L/t is 183–244 and 363–484, respectively. Therefore, if only the residual stress is responsible for the buckle delamination (like those discussed in previous sections of this paper), the effective membrane size r/t should be roughly 79–105 and 156–208, for petal and branched patterns, respectively. In what follows, we choose the representative effective r/t to be 100 and 200, respectively.

In order to qualitatively reproduce the morphology of buckle delamination in Ref. [21] using the current thin film membrane wrinkling model, besides the effective r/t we also need to determine the effective values of $E_{\text{out}}/E_{\text{in}}$ and σ_f/σ_c. Due to the very different system setup and buckling mechanisms, the estimation is fairly qualitative. First, the stiffness of the wafer should be many times higher than that of the membrane; we assume the effective $E_{\text{out}}/E_{\text{in}} = 40$ which is likely an underestimation. According to Lee et al. [21], $L_c \cdot \sigma_c^3$ is roughly a constant, where L_c is the critical delamination radius and σ_c the critical buckling stress. Therefore one may estimate that the normalized stress (σ_f/σ_c) is about 13.

With these assumed parameters, Fig. 7(e)–(f) gives the simulated patterns using the present model. These patterns qualitatively agree with experimental observations despite the distinct buckling mechanisms and system setup. Moreover, the wave numbers predicted from the present FEM simulations are 5 and 11, respectively, for petal and branched patterns, which are close to the experimental results, 6 and 12. We emphasize again that such an agreement may be due to error cancellation with the very crude assumptions made during the model comparison. Nevertheless, the current spontaneous buckling model of the constrained membrane thin film may provide some useful insight on the overall morphology of buckle delamination.

4 Concluding remarks

Motivated by the commonly observed wrinkling morphology of paper wetted by water drop, we study the wrinkles occurring in the center of a membrane thin sheet due to inhomogeneous deformation using finite element simulations. When the circular area inside a large thin film undergoes in-plane swelling, owing to the constraint imposed by the surrounding material an equibiaxial compression field is developed, and subsequently the system wrinkles. Depending on the three key parameters, the normalized expanding (inner) area size r/t, the modulus mismatch $E_{\text{out}}/E_{\text{in}}$, and the normalized stress σ_f/σ_c, ripple, petal, and branched patterns may emerge sequentially as the mismatch stress increases. The ripple-like pattern is favored at small r/t, $E_{\text{out}}/E_{\text{in}}$ and σ_f/σ_c, while the branched pattern is preferred at large values of r/t, $E_{\text{out}}/E_{\text{in}}$ and σ_f/σ_c; the petal pattern is a transition mode in-between and it may be extinct if r/t or $E_{\text{out}}/E_{\text{in}}$ is very high. For petal and branched patterns, at a given normalized stress level, the circumferential wrinkle number increases with the normalized inner area size and modulus mismatch. The maximum deflection of the wrinkle increases with r/t, $E_{\text{out}}/E_{\text{in}}$ and σ_f/σ_c. The model also sheds some qualitative light for explaining the overall morphology of delamination/blister patterns in

film/substrate systems, where despite the distinctive mechanisms, the present thin-film wrinkling model can, to some extent, reproduce the petal and branched delamination patterns at appropriate blister sizes and stress levels.

By following the unveiled mechanics principles, the wrinkling process of the constrained membrane thin film may provide useful hints for three-dimensional microfabrication, through controlled mechanical self-assembly and differential in-plane deformation [22–27]. The study may also provide insights for explaining the morphogenesis of certain natural or biological systems [18, 19, 22, 23, 28]. These topics will be subjected to future studies.

Acknowledgements The work is supported by National Natural Science Foundation of China (11172231), Independent Innovation Fund of Shandong University (2011GN055), DARPA (W91CRB-11-C-0112), World Class University program through the National Research Foundation of Korea (R32-2008-000-20042-0), Changjiang Scholar Program from Ministry of Education of China, and National Science Foundation (CMMI-0643726). YY and BW are funded by the China Scholarship Council.

References

1. T.A. Witten, Rev. Mod. Phys. **79**, 643 (2007)
2. J. Huang, M. Juszkiewicz, W.H. de Jeu, E. Cerda, T. Emrick, N. Menon, T.P. Russell, Science **317**, 650 (2007)
3. L. Pocivavsek, R. Dellsy, A. Kern, S. Johnson, B. Lin, K.Y.C. Lee, E. Cerda, Science **320**, 912 (2008)
4. T. Tallinen, J.A. Astrom, J. Timonen, Nat. Mater. **8**, 25 (2009)
5. G.A. Vliegenthart, G. Gompper, Nat. Mater. **5**, 216 (2006)
6. M.K. Small, W.D. Nix, J. Mater. Res. **7**, 1553 (1992)
7. Y. Xiang, X. Chen, J.J. Vlassak, J. Mater. Res. **20**, 2360 (2005)
8. H. Lee, B. Jung, D. Kim, H. Park, Int. J. Precis. Eng. Manuf. **12**, 865 (2011)
9. E. Cerda, L. Mahadevan, Phys. Rev. Lett. **90**, 074302 (2003)
10. E. Sharon, B. Roman, M. Marder, G. Shin, H.L. Swinney, Nature **419**, 579 (2002)
11. H. Liang, L. Mahadevan, Proc. Natl. Acad. Sci. USA **106**, 22049 (2009)
12. E. Sharon, B. Roman, H.L. Swinney, Phys. Rev. E **75**, 046211 (2007)
13. T. Mora, A. Boudaoud, Eur. Phys. J. E **20**, 119 (2006)
14. Z.S. Liu, W. Hong, Z.G. Suo, S. Swaddiwudhipong, Y.W. Zhang, Comput. Mater. Sci. **49**, S60 (2010)
15. Y. Klein, E. Efrati, E. Sharon, Science **315**, 1116 (2007)
16. E. Sharon, E. Efrati, Soft Mater. **6**, 5693 (2010)
17. S. Edmondson, K. Frieda, J.E. Comrie, P.R. Onck, W.T.S. Huck, Adv. Mater. **18**, 724 (2006)
18. J. Yin, Z. Cao, C. Li, I. Sheinman, X. Chen, Proc. Natl. Acad. Sci. **105**, 19132 (2008)
19. J. Yin, X. Chen, I. Sheinman, J. Mech. Phys. Solids **57**, 1470 (2009)
20. A.S. Argon, V. Gupta, H.S. Landis, J.A. Cornie, Mater. Sci. Eng. A **107**, 41 (1989)
21. K. Lee, S. Lee, D.-Y. Khang, T. Lee, Soft Mater. **6**, 3249 (2010)
22. X. Chen, J. Yin, Soft Mater. **6**, 5667 (2010)
23. H. Xiao, X. Chen, Soft Mater. **7**, 10794 (2011)
24. J. Yin, E. Bar-Kochba, X. Chen, Soft Mater. **5**, 3469 (2009)
25. J. Yin, X. Chen, J. Phys. D **43**, 115402 (2010)
26. J. Yin, X. Chen, J. Phys. D **44**, 045401 (2011)
27. J. Yin, X. Chen, Philos. Mag. Lett. **90**, 423 (2010)
28. J. Yin, G. Gerling, X. Chen, Acta Biomater. **6**, 1487 (2010)